JCTC Journal of Chemical Theory and Computation

Article

pubs.acs.org/JCTC

Electronic Properties of Zigzag Graphene Nanoribbons Studied by TAO-DFT

Chun-Shian Wu[†,‡] and Jeng-Da Chai*[,†,⊥,§]

[†]Department of Physics, [‡]Department of Chemistry, [⊥]Center for Theoretical Sciences and Center for Quantum Science and Engineering, and [§]Physics Division, National Center for Theoretical Sciences (North), National Taiwan University, Taipei 10617, Taiwan

Supporting Information

ABSTRACT: Accurate prediction of the electronic properties of zigzag graphene nanoribbons (ZGNRs) has been very challenging for conventional electronic structure methods due to the presence of strong static correlation effects. To meet the challenge, we study the singlet−triplet energy gaps, vertical ionization potentials, vertical electron affinities, fundamental gaps, and symmetrized von Neumann entropy (i.e., a measure of polyradical character) of hydrogen-terminated ZGNRs with different widths and lengths using our recently developed thermally-assisted-occupation density functional theory (TAO-DFT) [Chai, J.-D. *J. Chem. Phys.* **2012**, *136*, 154104], a very efficient method for the study of large strongly correlated systems. Our results are in good agreement with the available experimental and high-accuracy ab initio data. The ground states of ZGNRs are shown to be singlets for all the widths and lengths investigated. With the increase of ribbon length, the singlet−triplet energy gaps, vertical ionization potentials, and fundamental gaps decrease monotonically, while the vertical electron affinities and symmetrized von Neumann entropy increase monotonically. On the basis of the calculated orbitals and their occupation numbers, the longer ZGNRs are shown to possess increasing polyradical character in their ground states, where the active orbitals are mainly localized at the zigzag edges.

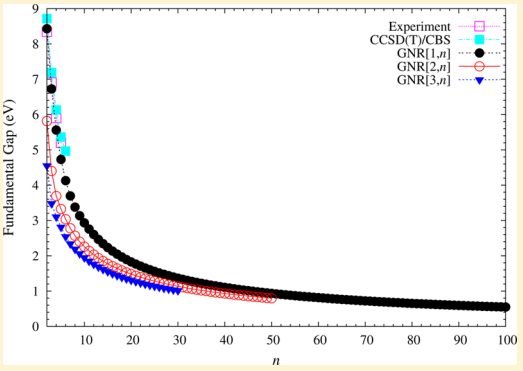

1. INTRODUCTION

The recent discovery of graphene, a single atomic plane of graphite, has attracted enormous interest owing to its fascinating properties and technological potential.[1−5] The high carrier mobility and long spin diffusion length of graphene offer the possibility of building promising graphene-based electronics and spintronics.[2,3] However, unlike the semiconductor silicon, graphene lacks an energy gap (i.e., band gap) between the valence and conduction bands and cannot be turned on and off for transistor applications. Exploring methods to open a band gap in graphene is essential for its potential electronic applications.

One way of introducing a band gap into graphene is to confine the carriers to quasi-one-dimensional systems, such as graphene nanoribbons (GNRs), which are long and narrow strips of graphene. Consequently, several methods have been proposed for the synthesis of GNRs.[6−9] Owing to their fascinating electronic and magnetic properties, GNRs have recently received considerable attention from many researchers,[10−50] bringing tremendous possibilities to realize electronic[27,28] and spintronic[18,23,29] nanodevices. Due to the pronounced quantum confinement and edge effects, the electronic properties of GNRs are strongly dependent on their geometrical structure, such as the width, length, and edge shape (zigzag, armchair, or chiral). Therefore, developing a comprehensive understanding of the relevant parameters controlling the electronic properties of GNRs is essentially important for the design of GNR-based nanodevices.

In spite of the increasing interest in GNRs, it remains very difficult to explore the electronic properties of long-chain GNRs from both experimental and theoretical perspectives. On the experimental side, the difficulties in synthesizing long-chain GNRs and their instability following isolation have been attributed to their radical character. Accordingly, there have been few reported measurements on long-chain GNRs.[46−50] On the theoretical side, GNRs, which belong to π-conjugated systems, typically require high-level ab initio multireference methods, such as the density matrix renormalization group (DMRG) algorithm,[26,40] the variational two-electron reduced density matrix (2-RDM) method,[36] or other high-level methods,[33−35,37,38,42,45] to accurately describe the strong static correlation effects. Nevertheless, these methods can be prohibitively expensive for the study of long-chain GNRs.

In contrast, Kohn−Sham density functional theory (KS-DFT)[51,52] has been one of the most popular methods for the study of ground-state properties of large systems, due to its favorable cost-to-performance ratio. However, its essential

Received: November 7, 2014

DOI: 10.1021/ct500999m
J. Chem. Theory Comput. XXXX, XXX, XXX−XXX

ingredient, the exact exchange-correlation (XC) functional, remains unknown and needs to be approximated. For systems with pronounced strong static correlation effects (i.e., strongly correlated (SC) systems), such as bond-breaking reactions, conjugated polymers, and transition-metal compounds, the predictions of semilocal density functionals, such as the local density approximation (LDA) and generalized gradient approximations (GGAs), can be problematic. Hybrid[53−60] and double-hybrid[61−69] density functionals may also yield erroneous results for SC systems.[70−72] Therefore, KS-DFT employing conventional (LDA, GGA, hybrid, and double-hybrid) functionals may no longer provide reliable results for long-chain GNRs, which should have the multireference character involving strong static correlation.[26,32,39−45]

Aiming to study the ground-state properties of large SC systems with minimum computational complexity, we have recently developed thermally-assisted-occupation density functional theory (TAO-DFT).[39] Unlike conventional ab initio multireference methods, the computational complexity of TAO-DFT increases very insignificantly with the size of the active space (i.e., an active space restriction is not needed for TAO-DFT calculations), showing that TAO-DFT can be very promising for the study of large polyradical systems, such as long-chain GNRs. In contrast to KS-DFT, TAO-DFT is a density functional theory with fractional orbital occupations produced by the Fermi−Dirac distribution (controlled by a fictitious temperature θ). However, existing XC functionals (e.g., LDA and GGAs) in KS-DFT may also be adopted in TAO-DFT.[43] TAO-DFT has similar computational cost as KS-DFT for single-point energy calculations and analytical nuclear gradients, and reduces to KS-DFT in the absence of strong static correlation effects. In addition, as discussed in ref 39, TAO-DFT offers an explicit description of strong static correlation via the entropy contribution (e.g., see eq 26 of ref 39). Even at the simplest LDA level, the resulting TAO-LDA has been shown to perform reasonably well for multireference systems (due to the appropriate treatment of static correlation), when the distribution of orbital occupation numbers (related to the chosen θ) is close to that of the natural orbital occupation numbers (NOONs).[73] However, this implies that a system-dependent θ (related to the distribution of NOONs) should be needed to capture the essential physics of strong static correlation effects. For simplicity, an optimal value of θ = 7 mhartree has been defined for TAO-LDA, based on the physical arguments and numerical investigations presented in ref 39. Interestingly, TAO-LDA (with θ = 7 mhartree) has been shown to consistently improve upon KS-LDA[74,75] for multireference systems, while performing similarly to KS-LDA for single-reference systems.

Due to its computational efficiency and reasonable accuracy for large systems with strong static correlation effects, in this work, we adopt TAO-LDA to study the electronic properties of zigzag GNRs (ZGNRs) with different widths and lengths. In particular, the availability of analytical nuclear gradients for TAO-LDA enables extremely efficient geometry optimization of molecules. Our results are compared with the available experimental and high-accuracy ab initio data as well as the results obtained from various density functionals in KS-DFT.

2. COMPUTATIONAL DETAILS

Here a series of polycyclic aromatic hydrocarbons (PAHs) are taken as finite-size models of ZGNRs. The ZGNRs considered have zigzag edges on both sides with hydrogen passivation. As illustrated in Figure 1, a rectangular GNR with width = m (in the armchair direction) and length = n (in the zigzag direction),

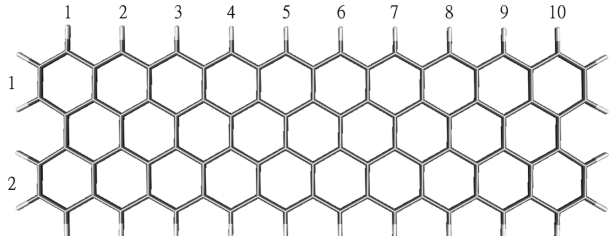

Figure 1. Rectangular graphene nanoribbon with width = 2 (in the armchair direction) and length = 10 (in the zigzag direction), designated as GNR[2, 10].

is designated as GNR[m, n]. Particularly, GNR[1, n] are linear n-acenes ($C_{4n+2}H_{2n+4}$), consisting of n linearly fused benzene rings, which have recently attracted significant attention from many experimental and theoretical researchers due to their novel electronic properties.[16,26,31−34,36−39,42−50] Note that the number of electrons in GNR[m, n] ($C_{4mn+2m}H_{4m+2n}$) is $24mn + 16m + 2n$, which can quickly increase with the increase of m and n.

To circumvent the formidable computational expense of high-level ab initio multireference methods, we investigate the singlet−triplet energy (ST) gaps, vertical ionization potentials, vertical electron affinities, fundamental gaps, and symmetrized von Neumann entropy of ZGNRs with three different widths and various lengths, involving GNR[1, n] (up to n = 100), GNR[2, n] (up to n = 50), and GNR[3, n] (up to n = 30), using KS-LDA[74,75] and TAO-LDA.[39] For all the TAO-LDA calculations, we adopt the optimal value of θ = 7 mhartree (as defined in ref 39). As KS-LDA is simply TAO-LDA (with θ = 0), it is important to examine the performance of KS-LDA here to assess the significance of TAO-LDA.

All calculations are performed with a development version of Q-Chem 4.0.[76] Results are computed using the 6-31G(d) basis set[77] with the fine grid EML(75, 302), consisting of 75 Euler−Maclaurin radial grid points[78] and 302 Lebedev angular grid points.[79] Spin-unrestricted KS-LDA and TAO-LDA calculations are performed for the lowest singlet and triplet energies of GNR[m, n] on the respective geometries that were fully optimized at the same level of theory. The ST gap of GNR[m, n] is calculated as ($E_T - E_S$), the energy difference between the lowest triplet (T) and singlet (S) states of GNR[m, n].

3. RESULTS AND DISCUSSION

Figure 2 shows the ST gaps of GNR[1, n] as a function of the ribbon length, calculated using spin-unrestricted KS-LDA and TAO-LDA. The results are compared with the available experimental data (uncorrected for zero-point vibrations, thermal vibrations, etc.)[46−49] and high-accuracy ab initio data calculated using the DMRG algorithm[26] and the coupled-cluster theory with iterative singles and doubles and perturbative treatment of triple substitutions at the complete basis set limit (CCSD(T)/CBS)[34] as well as the results obtained from the CAM-B3LYP functional[55] (a popular range-separated hybrid functional) in KS-DFT.[40] The ST gaps calculated using KS-LDA and CAM-B3LYP unexpectedly increase beyond GNR[1, 10] and GNR[1, 8], respectively, due to unphysical symmetry-breaking effects.[26,32,39−45] By contrast, the ST gaps calculated using TAO-LDA decrease

DOI: 10.1021/ct500999m
J. Chem. Theory Comput. XXXX, XXX, XXX−XXX

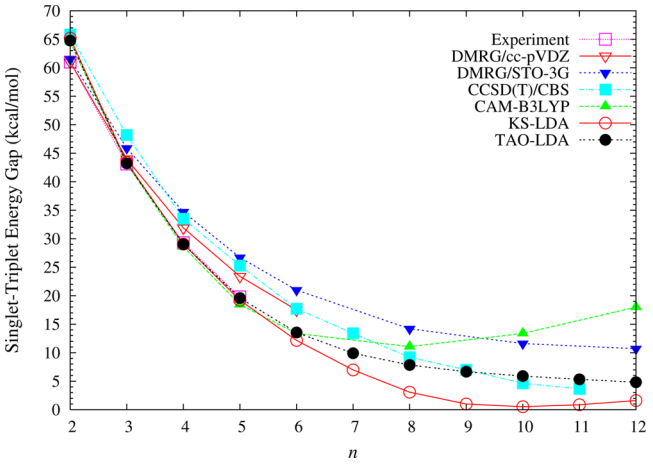

Figure 2. Singlet−triplet energy gap of GNR[1, n] as a function of the ribbon length, calculated using spin-unrestricted KS-LDA and TAO-LDA. For comparison, the experimental data (uncorrected for zero-point vibrations, thermal vibrations, etc.),[46−49] the DMRG data,[26] the CCSD(T)/CBS data,[34] and the CAM-B3LYP data[40] are taken from the literature.

monotonically with the increase of ribbon length, showing consistency with the experimental data and those calculated using the DMRG algorithm and CCSD(T)/CBS method.

Similar trends can be observed for GNR[2, n] (see Figure 3) and GNR[3, n] (see Figure 4), where the DMRG and CAM-

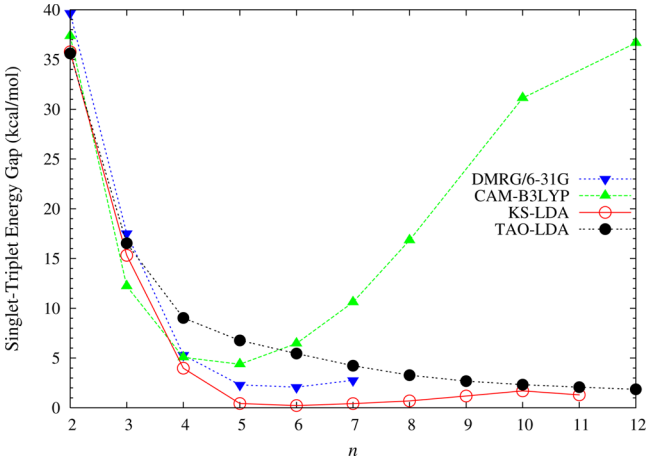

Figure 3. Singlet−triplet energy gap of GNR[2, n] as a function of the ribbon length, calculated using spin-unrestricted KS-LDA and TAO-LDA. For comparison, the DMRG and CAM-B3LYP data are taken from the work of Mizukami et al.[40]

B3LYP data are taken from the work of Mizukami et al.[40] for comparison. Note that if long-chain ZGNRs are to be reliably investigated by the DMRG algorithm, a sufficiently large number of renormalized basis states should be adopted, which can, however, be prohibitively expensive. As shown in Figure 3, the ST gaps calculated using the DMRG algorithm unexpectedly increase beyond GNR[2, 6], possibly due to the insufficient number of the renormalized basis states adopted in the calculations.[40]

To show the ribbon width effect on the ST gaps calculated using TAO-LDA, Figures 5 and 6 plot the ST gaps of GNR[1−3, n] as a function of the ribbon length. Based on our TAO-LDA calculations, the ST gaps decrease monotonically with

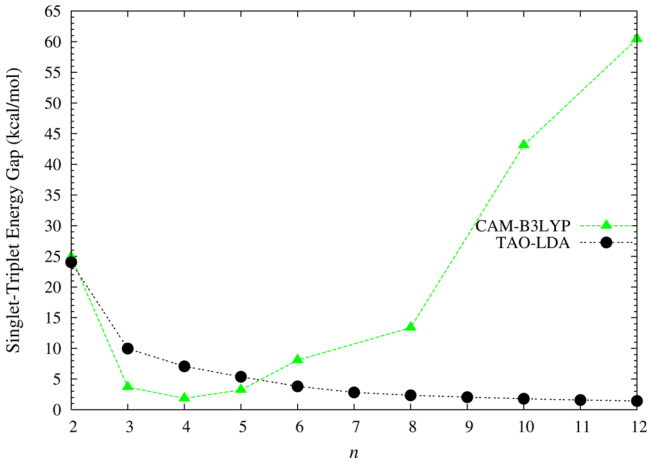

Figure 4. Singlet−triplet energy gap of GNR[3, n] as a function of the ribbon length, calculated using spin-unrestricted TAO-LDA. For comparison, the CAM-B3LYP data are taken from the work of Mizukami et al.[40]

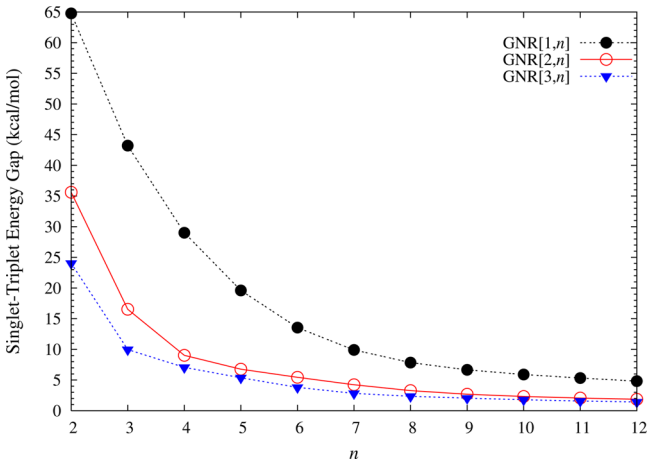

Figure 5. Singlet−triplet energy gap of GNR[1−3, n] as a function of the ribbon length, calculated using spin-unrestricted TAO-LDA.

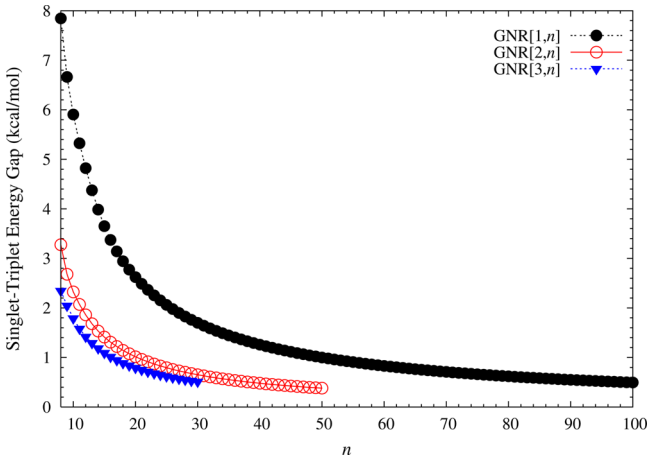

Figure 6. Same as in Figure 5, but for the longer GNR[1−3, n].

increasing ZGNR length for each ribbon width, and the ground states of ZGNRs are singlets for all the widths and lengths investigated.

Along the upper zigzag edge, the maximum C−C bond length difference between the lowest singlet and triplet states of

DOI: 10.1021/ct500999m
J. Chem. Theory Comput. XXXX, XXX, XXX−XXX

GNR[1−3, n] as a function of the ribbon length, calculated using spin-unrestricted TAO-LDA, are shown in Table 1.

Table 1. Along the Upper Zigzag Edge, the Maximum C−C Bond Length Difference (Å) between the Lowest Singlet and Triplet States of GNR[1−3, n] as a Function of the Ribbon Length, Calculated Using Spin-Unrestricted TAO-LDA

n	GNR[1, n]	GNR[2, n]	GNR[3, n]
2	0.052	0.018	0.009
4	0.025	0.004	0.002
6	0.015	0.001	0.001
8	0.005	0.001	0.001
10	0.002	0.001	0.000

Similar to previous findings,[16,31] the geometries for the lowest singlet and triplet states of GNR[1, n] become very similar for a sufficiently large n, supporting the absence of the Peierls distortion in this limit. For wider ZGNRs, the Peierls distortion vanishes more rapidly with increasing ribbon length.

Due to the symmetry constraint, the spin-restricted and spin-unrestricted energies for the lowest singlet state of GNR[m, n], calculated by the exact theory, should be identical.[39,41,43] To examine the possible symmetry-breaking effects, spin-restricted TAO-LDA calculations are also performed for the lowest singlet energies on the respective geometries that were fully optimized at the same level. Within the numerical precision considered in this work, the spin-restricted and spin-unrestricted TAO-LDA energies for the lowest singlet state of GNR[m, n] are essentially the same, and no spin density is numerically observed in spin-unrestricted TAO-LDA calculations, implying that essentially no unphysical symmetry-breaking effects occur in our spin-unrestricted TAO-LDA calculations.

At the optimized geometry of the lowest singlet state (i.e., the ground state) of GNR[m, n], containing N electrons, the vertical ionization potential $IP_v = E_{N-1} - E_N$, vertical electron affinity $EA_v = E_N - E_{N+1}$, and fundamental gap $E_g = IP_v - EA_v = E_{N+1} + E_{N-1} - 2E_N$ are obtained by multiple energy-difference calculations, where E_N is the total energy of the N-electron system. With the increase of ribbon length, IP_v (see Figure 7) monotonically decreases, and EA_v (see Figure 8) monotonically increases, yielding a monotonically deceasing E_g (see Figure 9). For GNR[1, n], our results are in good agreement with the available experimental data[50] and those calculated using the CCSD(T)/CBS method.[37,38] At the level of TAO-LDA, the E_g of the longest ZGNR studied for each ribbon width is 0.55 eV for GNR[1, 100], 0.80 eV for GNR[2, 50], and 1.02 eV for GNR[3, 30]. Note that the calculated E_g is within the most interesting range (1−3 eV) for GNR[1, n] (n: 46−10), GNR[2, n] (n: 36−7), and GNR[3, n] (n: 30−5), giving promise for applications of ZGNRs in nanophotonics.

To examine the possible polyradical character of GNR[m, n], as the orbital occupation numbers resulting from the TAO-LDA calculations are closely related to the NOONs,[73] we calculate the symmetrized von Neumann entropy (e.g., see eq 9 of ref 41)

$$S_{vN} = -\frac{1}{2}\sum_{i=1}^{\infty}\{f_i \ln(f_i) + (1-f_i)\ln(1-f_i)\} \quad (1)$$

for the lowest singlet state of GNR[m, n] as a function of the ribbon length, using spin-restricted TAO-LDA. Here f_i the occupation number of the ith orbital obtained with TAO-LDA, ranging from 0 to 1, is approximately equal to the occupation number of the ith natural orbital.[39,43] Note that S_{vN} essentially provides no contributions for a single-reference system ($\{f_i\}$ are close to either 0 or 1) and quickly increases with the number of active orbitals ($\{f_i\}$ are fractional for active orbitals and are close to either 0 or 1 for others). As shown in Figure 10, S_{vN} increases monotonically with the ribbon length.

To illustrate the causes of the increase of S_{vN} with ribbon length, we plot the active orbital occupation numbers for the lowest singlet state of GNR[1, n] (Figure 11), GNR[2, n] (Figure 12), and GNR[3, n] (Figure 13) as a function of the ribbon length, calculated using spin-restricted TAO-LDA. Here, the highest occupied molecular orbital (HOMO) is the (N/2)th orbital, and the lowest unoccupied molecular orbital (LUMO) is the (N/2 + 1)th orbital, with N being the number of electrons in GNR[m, n]. For brevity, HOMO, HOMO − 1, ..., and HOMO − 8, are denoted as H, H − 1, ..., and H − 8, respectively, while LUMO, LUMO + 1, ..., and LUMO + 8, are

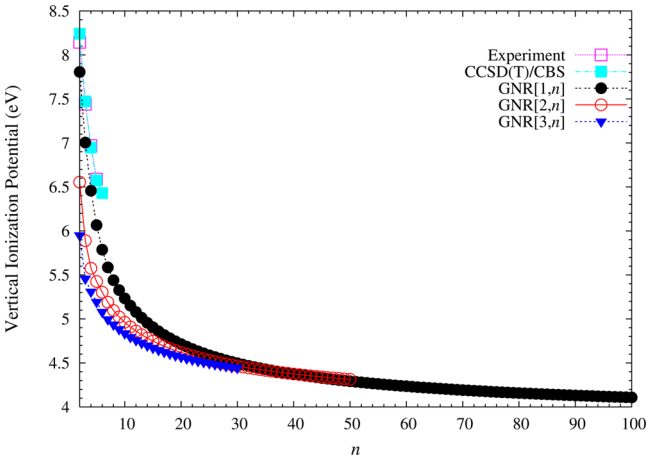

Figure 7. Vertical ionization potential for the lowest singlet state of GNR[1−3, n] as a function of the ribbon length, calculated using spin-unrestricted TAO-LDA. For GNR[1, n], the experimental data are taken from the compilation of Malloci et al.[50] and the CCSD(T)/CBS data are taken from the work of Deleuze et al.[37]

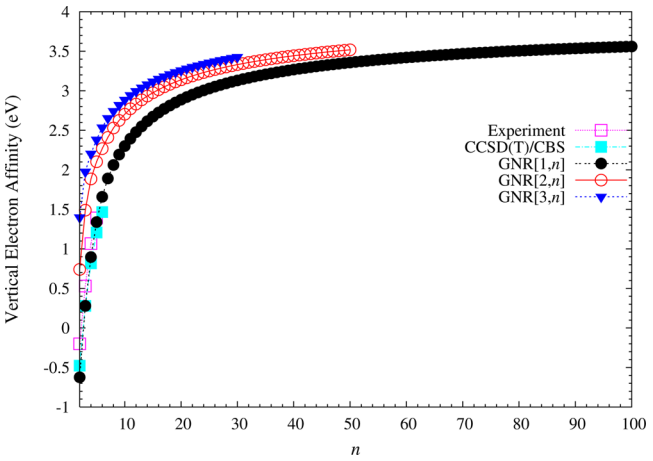

Figure 8. Vertical electron affinity for the lowest singlet state of GNR[1−3, n] as a function of the ribbon length, calculated using spin-unrestricted TAO-LDA. For GNR[1, n], the experimental data are taken from the compilation of Malloci et al.[50] and the CCSD(T)/CBS data are taken from Hajgató et al.[38]

DOI: 10.1021/ct500999m
J. Chem. Theory Comput. XXXX, XXX, XXX−XXX

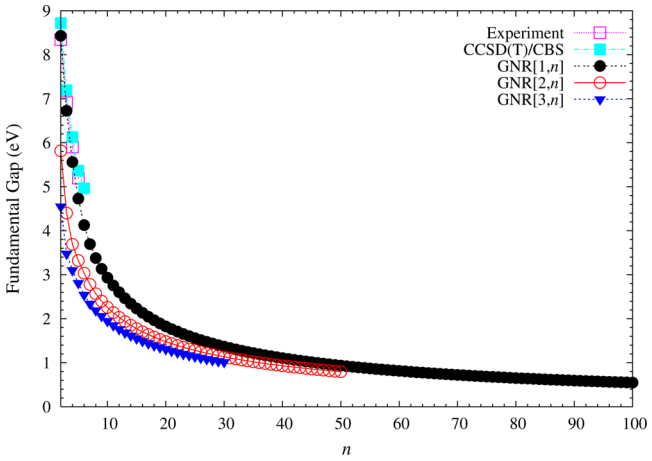

Figure 9. Fundamental gap for the lowest singlet state of GNR[1−3, n] as a function of the ribbon length, calculated using spin-unrestricted TAO-LDA. For GNR[1, n], the experimental data are taken from the compilation of Malloci et al.[50] and the CCSD(T)/CBS data are taken from Deleuze et al.[37] and Hajgató et al.[38]

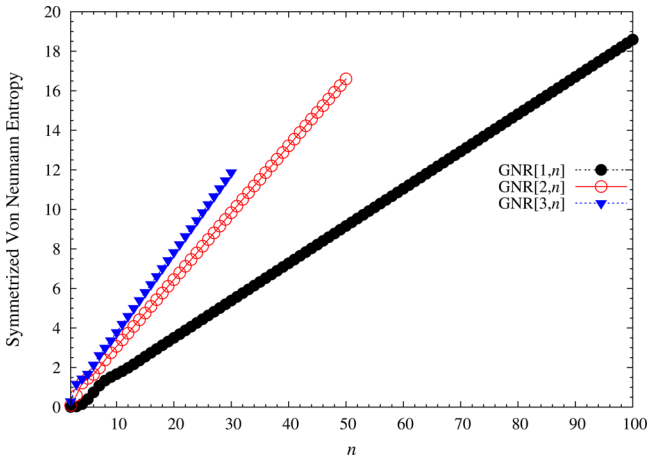

Figure 10. Symmetrized von Neumann entropy for the lowest singlet state of GNR[1−3, n] as a function of the ribbon length, calculated using spin-restricted TAO-LDA.

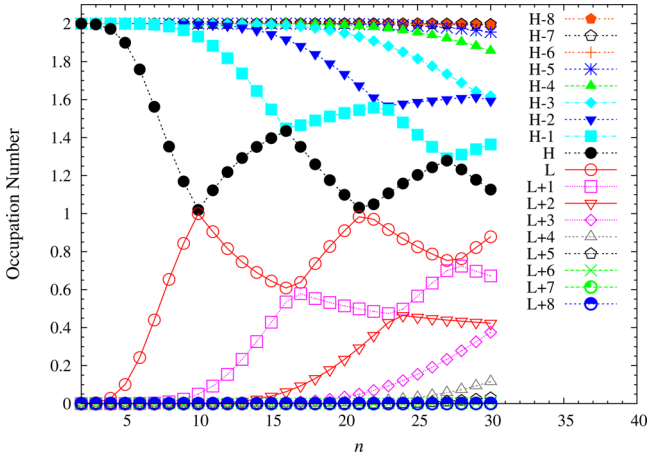

Figure 11. Active orbital occupation numbers (HOMO − 8, ..., HOMO − 1, HOMO, LUMO, LUMO + 1, ..., and LUMO + 8) for the lowest singlet state of GNR[1, n] as a function of the ribbon length, calculated using spin-restricted TAO-LDA.

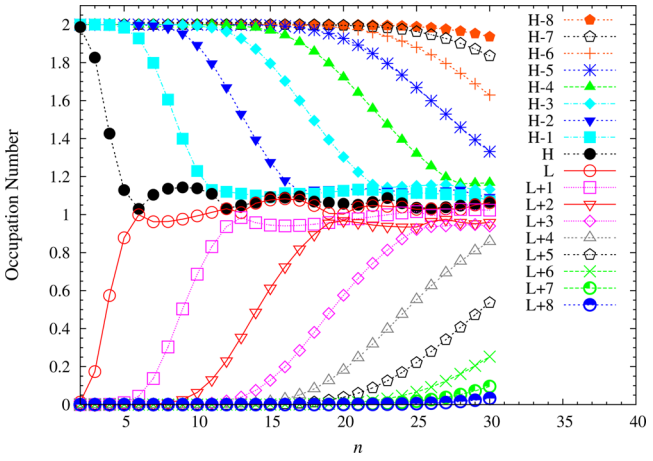

Figure 12. Active orbital occupation numbers (HOMO − 8, ..., HOMO − 1, HOMO, LUMO, LUMO + 1, ..., and LUMO + 8) for the lowest singlet state of GNR[2, n] as a function of the ribbon length, calculated using spin-restricted TAO-LDA.

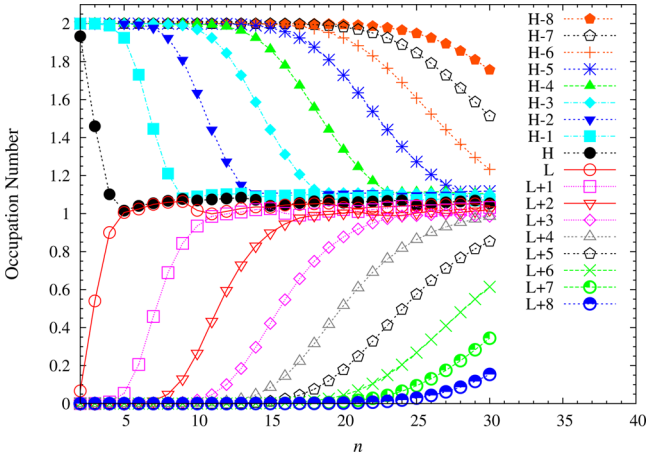

Figure 13. Active orbital occupation numbers (HOMO − 8, ..., HOMO − 1, HOMO, LUMO, LUMO + 1, ..., and LUMO + 8) for the lowest singlet state of GNR[3, n] as a function of the ribbon length, calculated using spin-restricted TAO-LDA.

denoted as L, L + 1, ..., and L + 8, respectively. As shown, the number of fractionally occupied orbitals increases with the increase of ribbon length, supporting the previous findings that ZGNRs with longer length should exhibit increasing polyradical character.[26,31,40−42,45] Similar to previous studies,[40−42,45] the evolution of polyradical character is more rapid for wider ZGNRs. Nevertheless, in contrast to previous studies,[26,40−42,45] the active orbital occupation numbers exhibit a curve crossing behavior in the approach to unity (singly occupied) with increasing ribbon length. For examples, the orbital with HOMO (LUMO) character in short-chain ZGNRs may become the LUMO (HOMO) in medium- to long-chain ZGNRs. Note that the curve crossing behavior may be an artifact showing the limitation of TAO-LDA (with a system-independent θ).

For the lowest singlet states of some representative GNR[m,n], we explore the real-space representation of active orbitals (those orbitals whose occupancy approaches to unity for sufficiently long ZGNRs), such as the HOMOs and LUMOs, obtained with spin-restricted TAO-LDA. As shown in Figures 14−16, our findings support previous research that the HOMO

DOI: 10.1021/ct500999m
J. Chem. Theory Comput. XXXX, XXX, XXX−XXX

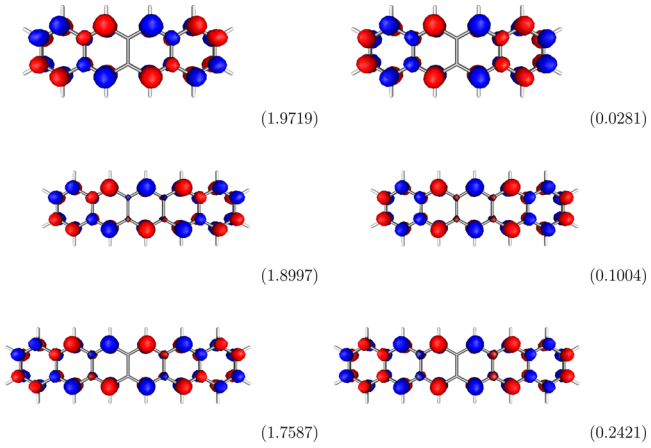

Figure 14. Real-space representation of the HOMOs (left) and LUMOs (right) for the lowest singlet states of GNR[1, 4], GNR[1, 5], and GNR[1, 6], calculated using spin-restricted TAO-LDA, at isovalue = 0.01 e/Å^3. The orbital occupation numbers are given in parentheses.

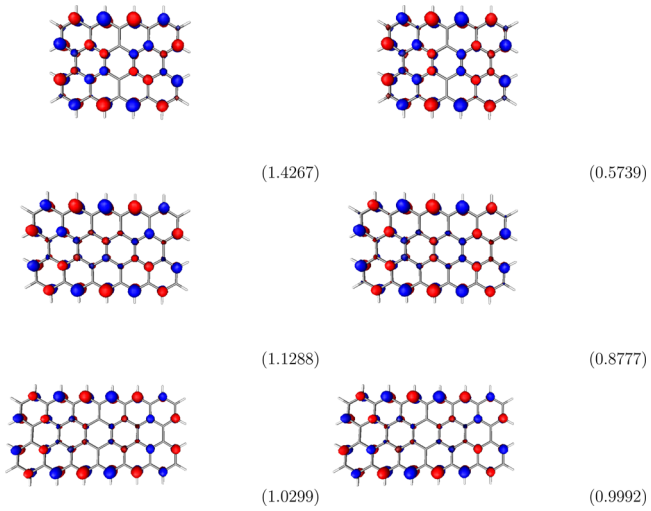

Figure 15. Real-space representation of the HOMOs (left) and LUMOs (right) for the lowest singlet states of GNR[2, 4], GNR[2, 5], and GNR[2, 6], calculated using spin-restricted TAO-LDA, at isovalue = 0.01 e/Å^3. The orbital occupation numbers are given in parentheses.

and LUMO of GNR[m, n] are mainly localized at the zigzag edges.[26,31,40,41] However, as discussed above, the orbital with HOMO (LUMO) character in GNR[2, 5] unexpectedly becomes the LUMO (HOMO) in GNR[2, 6]. Similar trends are also observed for those orbitals in GNR[3, 5] and GNR[3, 6].

4. CONCLUSIONS

In conclusion, we have presented a systematic computational study on the electronic properties (i.e., the ST gaps, vertical ionization potentials, vertical electron affinities, fundamental gaps, and symmetrized von Neumann entropy) of hydrogen-terminated ZGNRs with different widths and lengths using our recently developed TAO-LDA, a very efficient method for the study of large systems with strong static correlation effects. Our results are in good agreement with the available experimental and high-accuracy ab initio data. The ground states of ZGNRs have been shown to be singlets for all the widths and lengths investigated. With the increase of ZGNR length, the ST gaps, vertical ionization potentials, and fundamental gaps decrease

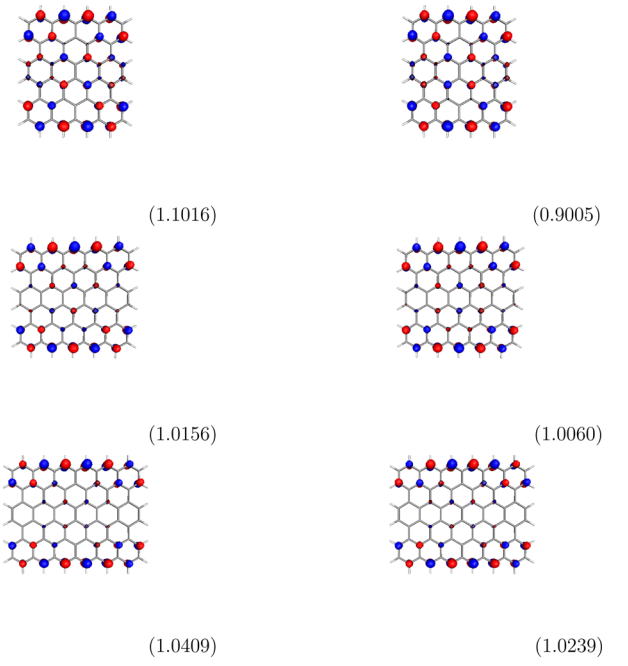

Figure 16. Real-space representation of the HOMOs (left) and LUMOs (right) for the lowest singlet states of GNR[3, 4], GNR[3, 5], and GNR[3, 6], calculated using spin-restricted TAO-LDA, at isovalue = 0.01 e/Å^3. The orbital occupation numbers are given in parentheses.

monotonically, while the vertical electron affinities and symmetrized von Neumann entropy increase monotonically. The effects of different ribbon widths on the electronic properties of ZGNRs have been presented and discussed. On the basis of the calculated orbitals and their occupation numbers, the longer ZGNRs should possess increasing polyradical character in their ground states, where the active orbitals are mainly localized at the zigzag edges. Although we have theoretically demonstrated that the electronic properties of GNRs can be manipulated with the appropriate choice of ribbon width and length, it remains to be addressed how these properties change with different edge types and chemical termination of the edges in GNRs. We intend to investigate these questions in the near future.

In view of the possible artifacts associated with the occupation numbers of TAO-LDA (with a system-independent θ), a system-dependent θ (related to the distribution of NOONs) is expected to improve the general performance of TAO-LDA and TAO-GGAs.[43] However, in situations where the self-interaction errors or noncovalent interaction errors of TAO-LDA or TAO-GGAs are pronounced, a fully nonlocal TAO-DFT [i.e., nonlocal XC functional and $E_\theta[\rho]$(see ref 39)] may be needed to resolve these failures.[39,43] We plan to investigate how to incorporate existing hybrid and double-hybrid density functionals into TAO-DFT to improve the accuracy of TAO-DFT for a wide range of single- and multireference systems.

■ ASSOCIATED CONTENT

Supporting Information

Detailed results for the electronic properties of hydrogen-terminated zigzag graphene nanoribbons with different widths and lengths are provided. This material is available free of charge via the Internet at http://pubs.acs.org/.

DOI: 10.1021/ct500999m
J. Chem. Theory Comput. XXXX, XXX, XXX−XXX

AUTHOR INFORMATION

Corresponding Author

*E-mail: jdchai@phys.ntu.edu.tw.

Notes

The authors declare no competing financial interest.

ACKNOWLEDGMENTS

This work was supported by the National Science Council of Taiwan (Grant No. NSC101-2112-M-002-017-MY3), National Taiwan University (Grant No. NTU-CDP-104R7855), the Center for Quantum Science and Engineering at NTU (Subproject Nos.: NTU-ERP-104R891401 and NTU-ERP-104R891403), and the National Center for Theoretical Sciences of Taiwan. We are grateful to the Computer and Information Networking Center at NTU for the partial support of high-performance computing facilities.

REFERENCES

(1) Novoselov, K. S.; Geim, A. K.; Morozov, S. V.; Jiang, D.; Zhang, Y.; Dubonos, S. V.; Grigorieva, I. V.; Firsov, A. A. Electric Field Effect in Atomically Thin Carbon Films. *Science* **2004**, *306*, 666−669.

(2) Novoselov, K. S.; Geim, A. K.; Morozov, S. V.; Jiang, D.; Katsnelson, M. I.; Grigorieva, I. V.; Dubonos, S. V.; Firsov, A. A. Two-Dimensional Gas of Massless Dirac Fermions in Graphene. *Nature* **2005**, *438*, 197−200.

(3) Zhang, Y.; Tan, Y.; Stormer, H. L.; Kim, P. Experimental Observation of the Quantum Hall Effect and Berry's Phase in Graphene. *Nature* **2005**, *438*, 201−204.

(4) Geim, A. K.; Novoselov, K. S. The Rise of Graphene. *Nat. Mater.* **2007**, *6*, 183−191.

(5) Geim, A. K. Graphene: Status and Prospects. *Science* **2009**, *324*, 1530−1534.

(6) Kosynkin, D. V.; Higginbotham, A. L.; Sinitskii, A.; Lomeda, J. R.; Dimiev, A.; Price, B. K.; Tour, J. M. Longitudinal Unzipping of Carbon Nanotubes to Form Graphene Nanoribbons. *Nature* **2009**, *458*, 872−876.

(7) Jiao, L.; Zhang, L.; Wang, X.; Diankov, G.; Dai, H. Narrow Graphene Nanoribbons from Carbon Nanotubes. *Nature* **2009**, *458*, 877−880.

(8) Cai, J.; Ruffieux, P.; Jaafar, R.; Bieri, M.; Braun, T.; Blankenburg, S.; Muoth, M.; Seitsonen, A. P.; Saleh, M.; Feng, X.; Müllen, K.; Fasel, R. Atomically Precise Bottom-Up Fabrication of Graphene Nanoribbons. *Nature* **2010**, *466*, 470−473.

(9) Talyzin, A. V.; Anoshkin, I. V.; Krasheninnikov, A. V.; Nieminen, R. M.; Nasibulin, A. G.; Jiang, H.; Kauppinen, E. I. Synthesis of Graphene Nanoribbons Encapsulated in Single-Walled Carbon Nanotubes. *Nano Lett.* **2011**, *11*, 4352−4356.

(10) Fujita, M.; Wakabayashi, K.; Nakada, K.; Kusakabe, K. Peculiar Localized State at Zigzag Graphite Edge. *J. Phys. Soc. Jpn.* **1996**, *65*, 1920−1923.

(11) Wakabayashi, K.; Sigrist, M.; Fujita, M. Spin Wave Mode of Edge-Localized Magnetic States in Nanographite Zigzag Ribbons. *J. Phys. Soc. Jpn.* **1998**, *67*, 2089−2093.

(12) Nakada, K.; Igami, M.; Fujita, M. Electron-Electron Interaction in Nanographite Ribbons. *J. Phys. Soc. Jpn.* **1998**, *67*, 2388−2394.

(13) Wakabayashi, K.; Fujita, M.; Ajiki, H.; Sigrist, M. Electronic and Magnetic Properties of Nanographite Ribbons. *Phys. Rev. B* **1999**, *59*, 8271.

(14) Kusakabe, K.; Maruyama, M. Magnetic Nanographite. *Phys. Rev. B* **2003**, *67*, 092406.

(15) Yamashiro, A.; Shimoi, Y.; Harigaya, K.; Wakabayashi, K. Spin- and Charge-Polarized States in Nanographene Ribbons with Zigzag Edges. *Phys. Rev. B* **2003**, *68*, 193410.

(16) Bendikov, M.; Duong, H. M.; Starkey, K.; Houk, K. N.; Carter, E. A.; Wudl, F. Oligoacenes: Theoretical Prediction of Open-Shell Singlet Diradical Ground States. *J. Am. Chem. Soc.* **2004**, *126*, 7416−7417.

(17) Lee, H.; Son, Y.-W.; Park, N.; Han, S.; Yu, J. Magnetic Ordering at the Edges of Graphitic Fragments: Magnetic Tail Interactions Between the Edge-Localized States. *Phys. Rev. B* **2005**, *72*, 174431.

(18) Son, Y.-W.; Cohen, M. L.; Louie, S. G. Half-Metallic Graphene Nanoribbons. *Nature* **2006**, *444*, 347−349.

(19) Son, Y.-W.; Cohen, M. L.; Louie, S. G. Energy Gaps in Graphene Nanoribbons. *Phys. Rev. Lett.* **2006**, *97*, 216803.

(20) Barone, V.; Hod, O.; Scuseria, G. E. Electronic Structure and Stability of Semiconducting Graphene Nanoribbons. *Nano Lett.* **2006**, *6*, 2748−2754.

(21) Yang, L.; Park, C.-H.; Son, Y.-W.; Cohen, M. L.; Louie, S. G. Quasiparticle Energies and Band Gaps in Graphene Nanoribbons. *Phys. Rev. Lett.* **2007**, *99*, 186801.

(22) Areshkin, D. A.; Gunlycke, D.; White, C. T. Ballistic Transport in Graphene Nanostrips in the Presence of Disorder: Importance of Edge Effects. *Nano Lett.* **2007**, *7*, 204−210.

(23) Rudberg, E.; Salek, P.; Luo, Y. Nonlocal Exchange Interaction Removes Half-Metallicity in Graphene Nanoribbons. *Nano Lett.* **2007**, *7*, 2211−2213.

(24) Hod, O.; Barone, V.; Peralta, J. E.; Scuseria, G. E. Enhanced Half-Metallicity in Edge-Oxidized Zigzag Graphene Nanoribbons. *Nano Lett.* **2007**, *7*, 2295−2299.

(25) Jiang, D.; Sumpter, B. G.; Dai, S. Unique Chemical Reactivity of a Graphene Nanoribbon's Zigzag Edge. *J. Chem. Phys.* **2007**, *126*, 134701.

(26) Hachmann, J.; Dorando, J. J.; Aviles, M.; Chan, G. K. L. The Radical Character of the Acenes: A Density Matrix Renormalization Group Study. *J. Chem. Phys.* **2007**, *127*, 134309.

(27) Han, M. Y.; Özyilmaz, B.; Zhang, Y.; Kim, P. Energy Band-Gap Engineering of Graphene Nanoribbons. *Phys. Rev. Lett.* **2007**, *98*, 206805.

(28) Özyilmaz, B.; Jarillo-Herrero, P.; Efetov, D.; Abanin, D. A.; Levitov, L. S.; Kim, P. Electronic Transport and Quantum Hall Effect in Bipolar Graphene p-n-p Junctions. *Phys. Rev. Lett.* **2007**, *99*, 166804.

(29) Yazyev, O. V.; Katsnelson, M. I. Magnetic Correlations at Graphene Edges: Basis for Novel Spintronics Devices. *Phys. Rev. Lett.* **2008**, *100*, 047209.

(30) Hod, O.; Barone, V.; Scuseria, G. E. Half-Metallic Graphene Nanodots: A Comprehensive First-Principles Theoretical Study. *Phys. Rev. B* **2008**, *77*, 035411.

(31) Jiang, D.; Dai, S. Electronic Ground State of Higher Acenes. *J. Phys. Chem. A* **2008**, *112*, 332−335.

(32) Casanova, D.; Head-Gordon, M. Restricted Active Space Spin-Flip Configuration Interaction Approach: Theory, Implementation and Examples. *Phys. Chem. Chem. Phys.* **2009**, *11*, 9779−9790.

(33) Hajgató, B.; Szieberth, D.; Geerlings, P.; De Proft, F.; Deleuze, M. S. A Benchmark Theoretical Study of the Electronic Ground State and of the Singlet-Triplet Split of Benzene and Linear Acenes. *J. Chem. Phys.* **2009**, *131*, 224321.

(34) Hajgató, B.; Huzak, M.; Deleuze, M. S. Focal Point Analysis of the Singlet-Triplet Energy Gap of Octacene and Larger Acenes. *J. Phys. Chem. A* **2011**, *115*, 9282−9293.

(35) Huzak, M.; Deleuze, M. S.; Hajgató, B. Half-Metallicity and Spin-Contamination of the Electronic Ground State of Graphene Nanoribbons and Related Systems: An Impossible Compromise? *J. Chem. Phys.* **2011**, *135*, 104704.

(36) Pelzer, K.; Greenman, L.; Gidofalvi, G.; Mazziotti, D. A. Strong Correlation in Acene Sheets from the Active-Space Variational Two-Electron Reduced Density Matrix Method: Effects of Symmetry and Size. *J. Phys. Chem. A* **2011**, *115*, 5632−5640.

(37) Deleuze, M. S.; Claes, L.; Kryachko, E. S.; François, J.-P. Benchmark Theoretical Study of the Ionization Threshold of Benzene and Oligoacenes. *J. Chem. Phys.* **2003**, *119*, 3106.

(38) Hajgató, B.; Deleuze, M. S.; Tozer, D. J.; De Proft, F. A Benchmark Theoretical Study of the Electron Affinities of Benzene and Linear Acenes. *J. Chem. Phys.* **2008**, *129*, 084308.

(39) Chai, J.-D. Density Functional Theory with Fractional Orbital Occupations. *J. Chem. Phys.* **2012**, *136*, 154104.

DOI: 10.1021/ct500999m
J. Chem. Theory Comput. XXXX, XXX, XXX−XXX

(40) Mizukami, W.; Kurashige, Y.; Yanai, T. More π Electrons Make a Difference: Emergence of Many Radicals on Graphene Nanoribbons Studied by Ab Initio DMRG Theory. *J. Chem. Theory Comput.* **2013**, *9*, 401−407.
(41) Rivero, P.; Jiménez-Hoyos, C. A.; Scuseria, G. E. Entanglement and Polyradical Character of Polycyclic Aromatic Hydrocarbons Predicted by Projected Hartree-Fock Theory. *J. Phys. Chem. B* **2013**, *117*, 12750−12758.
(42) Plasser, F.; Pašalić, H.; Gerzabek, M. H.; Libisch, F.; Reiter, R.; Burgdörfer, J.; Müller, T.; Shepard, R.; Lischka, H. The Multiradical Character of One- and Two-Dimensional Graphene Nanoribbons. *Angew. Chem., Int. Ed.* **2013**, *52*, 2581−2584.
(43) Chai, J.-D. Thermally-Assisted-Occupation Density Functional Theory with Generalized-Gradient Approximations. *J. Chem. Phys.* **2014**, *140*, 18A521.
(44) Small, D. W.; Lawler, K. V.; Head-Gordon, M. Coupled Cluster Valence Bond Method: Efficient Computer Implementation and Application to Multiple Bond Dissociations and Strong Correlations in the Acenes. *J. Chem. Theory Comput.* **2014**, *10*, 2027−2040.
(45) Horn, S.; Plasser, F.; Müller, T.; Libisch, F.; Burgdörfer, J.; Lischka, H. A Comparison of Singlet and Triplet States for One- and Two-Dimensional Graphene Nanoribbons using Multireference Theory. *Theor. Chem. Acc.* **2014**, *133*, 1511.
(46) Birks, J. B. *Photophysics of Aromatic Molecules*; Wiley: London, 1970; pp 142−300.
(47) Schiedt, J.; Weinkauf, R. Photodetachment Photoelectron Spectroscopy of Mass Selected Anions: Anthracene and the Anthracene-H_2O Cluster. *Chem. Phys. Lett.* **1997**, *266*, 201−205.
(48) Sabbatini, N.; Indelli, M. T.; Gandolfi, M. T.; Balzani, V. Quenching of Singlet and Triplet Excited States of Aromatic Molecules by Europium Ions. *J. Phys. Chem.* **1982**, *86*, 3585−3591.
(49) Burgos, J.; Pope, M.; Swenberg, Ch. E.; Alfano, R. R. Heterofission in Pentacene-Doped Tetracene Single Crystals. *Phys. Status Solidi B* **1977**, *83*, 249−256.
(50) Malloci, G.; Mulas, G.; Cappellini, G.; Joblin, C. Time-Dependent Density Functional Study of the Electronic Spectra of Oligoacenes in the Charge States −1, 0, +1, and +2. *Chem. Phys.* **2007**, *340*, 43−58.
(51) Hohenberg, P.; Kohn, W. Inhomogeneous Electron Gas. *Phys. Rev.* **1964**, *136*, B864.
(52) Kohn, W.; Sham, L. J. Self-Consistent Equations Including Exchange and Correlation Effects. *Phys. Rev.* **1965**, *140*, A1133.
(53) Becke, A. D. Density-Functional Thermochemistry. III. The Role of Exact Exchange. *J. Chem. Phys.* **1993**, *98*, 5648−5652.
(54) Iikura, H.; Tsuneda, T.; Yanai, T.; Hirao, K. A Long-Range Correction Scheme for Generalized-Gradient-Approximation Exchange Functionals. *J. Chem. Phys.* **2001**, *115*, 3540−3544.
(55) Yanai, T.; Tew, D. P.; Handy, N. C. A New Hybrid Exchange-Correlation Functional Using the Coulomb-Attenuating Method (CAM-B3LYP). *Chem. Phys. Lett.* **2004**, *393*, 51−57.
(56) Vydrov, O. A.; Heyd, J.; Krukau, A. V.; Scuseria, G. E. Importance of Short-Range versus Long-Range Hartree-Fock Exchange for the Performance of Hybrid Density Functionals. *J. Chem. Phys.* **2006**, *125*, 074106.
(57) Chai, J.-D.; Head-Gordon, M. Systematic Optimization of Long-Range Corrected Hybrid Density Functionals. *J. Chem. Phys.* **2008**, *128*, 084106.
(58) Chai, J.-D.; Head-Gordon, M. Long-Range Corrected Hybrid Density Functionals with Damped Atom-Atom Dispersion Corrections. *Phys. Chem. Chem. Phys.* **2008**, *10*, 6615−6620.
(59) Lin, Y.-S.; Tsai, C.-W.; Li, G.-D.; Chai, J.-D. Long-Range Corrected Hybrid Meta-Generalized-Gradient Approximations with Dispersion Corrections. *J. Chem. Phys.* **2012**, *136*, 154109.
(60) Lin, Y.-S.; Li, G.-D.; Mao, S.-P.; Chai, J.-D. Long-Range Corrected Hybrid Density Functionals with Improved Dispersion Corrections. *J. Chem. Theory Comput.* **2013**, *9*, 263−272.
(61) Grimme, S. Semiempirical Hybrid Density Functional with Perturbative Second-Order Correlation. *J. Chem. Phys.* **2006**, *124*, 034108.
(62) Chai, J.-D.; Head-Gordon, M. Long-Range Corrected Double-Hybrid Density Functionals. *J. Chem. Phys.* **2009**, *131*, 174105.
(63) Zhang, I. Y.; Xu, X.; Goddard, W. A., III Doubly Hybrid Density Functional for Accurate Descriptions of Nonbond Interactions, Thermochemistry and Thermochemical Kinetics. *Proc. Natl. Acad. Sci. U.S.A.* **2009**, *106*, 4963−4968.
(64) Sharkas, K.; Toulouse, J.; Savin, A. Double-Hybrid Density-Functional Theory Made Rigorous. *J. Chem. Phys.* **2011**, *134*, 064113.
(65) Brémond, E.; Adamo, C. Seeking for Parameter-Free Double-Hybrid Functionals: The PBE0-DH Model. *J. Chem. Phys.* **2011**, *135*, 024106.
(66) Toulouse, J.; Sharkas, K.; Brémond, E.; Adamo, C. Communication: Rationale for a New Class of Double-Hybrid Approximations in Density-Functional Theory. *J. Chem. Phys.* **2011**, *135*, 101102.
(67) Chai, J.-D.; Mao, S.-P. Seeking for Reliable Double-Hybrid Density Functionals without Fitting Parameters: The PBE0−2 Functional. *Chem. Phys. Lett.* **2012**, *538*, 121−125.
(68) Zhang, I. Y.; Xu, X. Reaching a Uniform Accuracy for Complex Molecular Systems: Long-Range-Corrected XYG3 Doubly Hybrid Density Functional. *J. Phys. Chem. Lett.* **2013**, *4*, 1669−1675.
(69) Su, N. Q.; Xu, X. Construction of a Parameter-Free Doubly Hybrid Density Functional from Adiabatic Connection. *J. Chem. Phys.* **2014**, *140*, 18A512.
(70) Kümmel, S.; Kronik, L. Orbital-Dependent Density Functionals: Theory and Applications. *Rev. Mod. Phys.* **2008**, *80*, 3.
(71) Cohen, A. J.; Mori-Sánchez, P.; Yang, W. Insights into Current Limitations of Density Functional Theory. *Science* **2008**, *321*, 792−794.
(72) Cohen, A. J.; Mori-Sánchez, P.; Yang, W. Challenges for Density Functional Theory. *Chem. Rev.* **2011**, *112*, 289−320.
(73) Löwdin, P.-O.; Shull, H. Natural Orbitals in the Quantum Theory of Two-Electron Systems. *Phys. Rev.* **1956**, *101*, 1730.
(74) Dirac, P. A. M. Note on Exchange Phenomena in the Thomas-Fermi Atom. *Proc. Cambridge Philos. Soc.* **1930**, *26*, 376−385.
(75) Perdew, J. P.; Wang, Y. Accurate and Simple Analytic Representation of the Electron-Gas Correlation Energy. *Phys. Rev. B* **1992**, *45*, 13244.
(76) Shao, Y.; Gan, Z.; Epifanovsky, E.; Gilbert, A. T. B.; Wormit, M.; Kussmann, J.; Lange, A. W.; Behn, A.; Deng, J.; Feng, X.; Ghosh, D.; Goldey, M.; Horn, P. R.; Jacobson, L. D.; Kaliman, I.; Khaliullin, R. Z.; Kuś, T.; Landau, A.; Liu, J.; Proynov, E. I.; Rhee, Y. M.; Richard, R. M.; Rohrdanz, M. A.; Steele, R. P.; Sundstrom, E. J.; Woodcock, H. L., III; Zimmerman, P. M.; Zuev, D.; Albrecht, B.; Alguire, E.; Austin, B.; Beran, G. J. O.; Bernard, Y. A.; Berquist, E.; Brandhorst, K.; Bravaya, K. B.; Brown, S. T.; Casanova, D.; Chang, C.-M.; Chen, Y.; Chien, S. H.; Closser, K. D.; Crittenden, D. L.; Diedenhofen, M.; DiStasio, R. A.; Do, H.; Dutoi, A. D.; Edgar, R. G.; Fatehi, S.; Fusti-Molnar, L.; Ghysels, A.; Golubeva-Zadorozhnaya, A.; Gomes, J.; Hanson-Heine, M. W. D.; Harbach, P. H. P.; Hauser, A. W.; Hohenstein, E. G.; Holden, Z. C.; Jagau, T.-C.; Ji, H.; Kaduk, B.; Khistyaev, K.; Kim, J.; Kim, J.; King, R. A.; Klunzinger, P.; Kosenkov, D.; Kowalczyk, T.; Krauter, C. M.; Lao, K. U.; Laurent, A.; Lawler, K. V.; Levchenko, S. V.; Lin, C. Y.; Liu, F.; Livshits, E.; Lochan, R. C.; Luenser, A.; Manohar, P.; Manzer, S. F.; Mao, S.-P.; Mardirossian, N.; Marenich, A. V.; Maurer, S. A.; Mayhall, N. J.; Neuscamman, E.; Oana, C. M.; Olivares-Amaya, R.; O'Neill, D. P.; Parkhill, J. A.; Perrine, T. M.; Peverati, R.; Prociuk, A.; Rehn, D. R.; Rosta, E.; Russ, N. J.; Sharada, S. M.; Sharma, S.; Small, D. W.; Sodt, A.; Stein, T.; Stück, D.; Su, Y.-C.; Thom, A. J. W.; Tsuchimochi, T.; Vanovschi, V.; Vogt, L.; Vydrov, O.; Wang, T.; Watson, M. A.; Wenzel, J.; White, A.; Williams, C. F.; Yang, J.; Yeganeh, S.; Yost, S. R.; You, Z.-Q.; Zhang, I. Y.; Zhang, X.; Zhao, Y.; Brooks, B. R.; Chan, G. K. L.; Chipman, D. M.; Cramer, C. J.; Goddard, W. A., III; Gordon, M. S.; Hehre, W. J.; Klamt, A.; Schaefer, H. F., III; Schmidt, M. W.; Sherrill, C. D.; Truhlar, D. G.; Warshel, A.; Xu, X.; Aspuru-Guzik, A.; Baer, R.; Bell, A. T.; Besley, N. A.; Chai, J.-D.; Dreuw, A.; Dunietz, B. D.; Furlani, T. R.; Gwaltney, S. R.; Hsu, C.-P.; Jung, Y.; Kong, J.; Lambrecht, D. S.; Liang, W. Z.; Ochsenfeld, C.; Rassolov, V. A.; Slipchenko, L. V.; Subotnik, J. E.; van Voorhis, T.;

DOI: 10.1021/ct500999m
J. Chem. Theory Comput. XXXX, XXX, XXX−XXX

Herbert, J. M.; Krylov, A. I.; Gill, P. M. W.; Head-Gordon, M. Advances in Molecular Quantum Chemistry Contained in the Q-Chem 4 Program Package. *Mol. Phys.* **2015**, *113*, 184−215.
(77) Krishnan, R.; Binkley, J. S.; Seeger, R.; Pople, J. A. Self-Consistent Molecular Orbital Methods. XX. A Basis Set for Correlated Wave Functions. *J. Chem. Phys.* **1980**, *72*, 650.
(78) Murray, C. W.; Handy, N. C.; Laming, G. J. Quadrature Schemes for Integrals of Density Functional Theory. *Mol. Phys.* **1993**, *78*, 997−1014.
(79) Lebedev, V. I.; Laikov, D. N. A Quadrature Formula for the Sphere of the 131st Algebraic Order of Accuracy. *Dokl. Math.* **1999**, *59*, 477−481.

DOI: 10.1021/ct500999m
J. Chem. Theory Comput. XXXX, XXX, XXX−XXX